Hierarchical Self-Assembly and Multidynamic Responsiveness of Fluorescent Dynamic Covalent Networks Forming Organogels

Esteban Suárez-Picado, Maëva Coste, Jean-Yves Runser, Mathieu Fossépré, Alain Carvalho, Mathieu Surin,* Loïc Jierry,* and Sébastien Ulrich*

Cite This: *Biomacromolecules* 2022, 23, 431−442

Read Online

ACCESS | Metrics & More | Article Recommendations | Supporting Information

ABSTRACT: Smart stimuli-responsive fluorescent materials are of interest in the context of sensing and imaging applications. In this project, we elaborated multidynamic fluorescent materials made of a tetraphenylethene fluorophore displaying aggregation-induced emission and short cysteine-rich C-hydrazide peptides. Specifically, we show that a hierarchical dynamic covalent self-assembly process, combining disulfide and acyl-hydrazone bond formation operating simultaneously in a one-pot reaction, yields cage compounds at low concentration (2 mM), while soluble fluorescent dynamic covalent networks and even chemically cross-linked fluorescent organogels are formed at higher concentrations. The number of cysteine residues in the peptide sequence impacts directly the mechanical properties of the resulting organogels, Young's moduli varying

2500-fold across the series. These materials underpinned by a nanofibrillar network display multidynamic responsiveness following concentration changes, chemical triggers, as well as light irradiation, all of which enable their controlled degradation with concomitant changes in spectroscopic outputs—self-assembly enhances fluorescence emission by ca. 100-fold and disassembly quenches fluorescence emission.
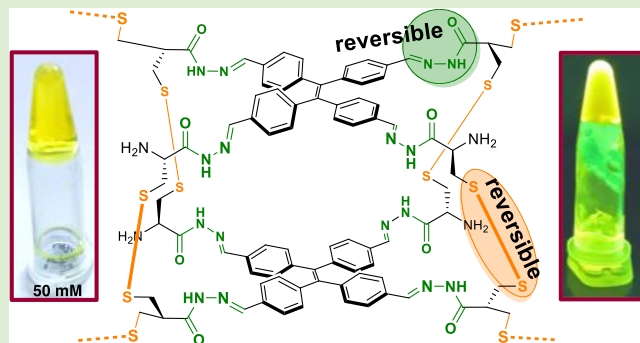
INTRODUCTION

Dynamic covalent chemistry is an innovative approach for designing smart (bio) materials in a bottom-up manner by crossing several length scales during the hierarchical self-assembly process.[1,2] This covalent self-assembly approach has already been successfully applied for making discrete entities such as shape-persistent macrocycles and molecular cages,[3] dynamic covalent polymers,[4−8] and higher-order dynamic covalent networks (DCNs).[9,10,3,11] These DCNs, which for instance can form functional gels, have attracted interest as smart soft materials.[12,13]

The reactional dynamics of the reversible covalent bond formation grants a fine control by temperature, solvent, and catalyst over the covalent self-assembly and thus enables tuning of the emerging mechanical properties—examples being reported with imines,[14] acyl-hydrazones,[15−17] and disulfides.[5,18−20] In addition, the reversible nature of these covalent linkages endows responsiveness to different kinds of physicochemical stimuli: light,[21,22] pH,[23,24] redox,[25] and mechanochemical activation.[26−29] This particular feature is a leverage tool for fabricating smart materials capable of controlled degradation,[30] self-healing,[9,31,32] and chemical recycling.[33]

In this context, borrowing ideas both from supramolecular chemistry[34] and synthetic organic chemistry,[35] the introduc-
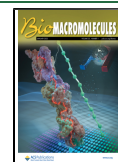
tion of multiple dynamic covalent linkages should facilitate the bottom-up self-assembly of complex networks, provided their reactivity is well mastered in order to funnel the process toward the formation of a unique material. Sets of reversible orthogonal covalent reactions and conditions have been recently found to enable their simultaneous operation toward the bottom-up fabrication of larger entities.[36] However, to date, only a few examples have tackled this challenge for making smart materials,[37−39] for instance combining acyl-hydrazones and disulfides or imines and Diels−Alder reactions in self-healing hydrogels[37,40] or oximes and boronate esters in self-healing materials.[41]

We have recently described the formation of fluorescent cages through such a one-pot combination of two reversible reactions that operate simultaneously: acyl-hydrazone and disulfide bond formation. Interestingly, these cages undergo a fluorescence emission enhancement and decrease upon, respectively, formation and chemically controlled dissocia-

tion.[42] Herein, we report our investigation of the subsequent hierarchical self-assembly of these fluorescent cages into responsive DCNs. We describe simple short cysteine-rich C-hydrazide peptides, which can be used as cross-linking building blocks, and characterize the formation of DCNs, which resulted in brightly fluorescent organogels that undergo controlled degradation triggered by component exchange, redox, and light stimuli.

■ MATERIALS AND METHODS

All reagents and solvents were obtained from commercial sources and were used without further purification.

Nuclear Magnetic Resonance (NMR). NMR experiments were measured in deuterated solvents at 400 MHz for ^{1}H and 100 MHz for ^{13}C (Bruker Avance 400 instruments) for proton NMR and 100 MHz for carbon. Peaks were referenced in ppm with respect to the residual solvent peak (CDCl$_3$: δ = 77.2 ppm; DMSO-d$_6$: δ = 39.5 ppm). Data are reported as follows: chemical shift (δ in ppm), multiplicity (s for singlet, d for doublet, t for triplet, and m for multiplet), coupling constant (J in hertz), and integration.

High-Performance Liquid Chromatography (HPLC). Analytical reverse-phase HPLC (RP-HPLC) analyses were performed on a Thermo Scientific HPLC Dionex UltiMate 3000 (Phenomenex Kinetex C18, 2.6 μm × 7.5 cm, 100 Å) with the following linear gradients of solvent B (acetonitrile 100%) into solvent A (H$_2$O 95% and acetonitrile 5%): Method: 0−95% of solvent B in 5 min; flow: 1 mL/min. Preparative HPLC was performed on (i) a Waters Prep LC Controller HPLC (XSelect CSH Prep C18, 5 μm, 250 × 30 mm column, Macherey-Nagel) equipped with a Waters 2489 detector, flow 30 mL/min, or on (ii) a VWR International LaPrep pump P110, a VWR LaPrep P314 Dual l absorbance detector, and EZChrom software (15 C18 reversed-phase column Waters Xbridge, RP-18, 250 × 25 mm, 5 μm), flow 40 mL/min, using a linear gradient mode elution: (i) for ^{Prot}C$_2$-Hyd and ^{Prot}CG$_n$C-Hyd (n = 1−3) from A = 95% initially to A = 50% at 30 min, then A = 5% for 15 min and (ii) for ^{Prot}C$_n$-Hyd (n = 3−4) from A = 80% initially to A = 50% at 30 min, then A = 5% for 15 min. HPLC eluents: Solution A: 99.9% water and 0.1% TFA; Solution B: 99.9% acetonitrile and 0.1% TFA.

Liquid Chromatography-Mass Spectrometry (LC/MS). Analyses were performed on a Shimadzu LCMS-2020 (Phenomenex Kinetex C18, 2.6 μm × 7.5 cm, 100 Å) equipped with an SPD-M20A detector with the following linear gradient of solvent B (99.9% acetonitrile and 0.1% HCOOH) and solvent A (99.9% water and 0.1% HCOOH): 5 to 95% of solvent B in 5 min; flow 1 mL/min. Retention times (t_R) are given in minutes.

Mass Spectrometry (MS). Electrospray ionization (ESI-MS) analyses were carried out at the Laboratoire de Mesures Physiques, IBMM, Université de Montpellier using Micromass Q-Tof instruments.

Solid Phase Peptide Synthesis (SPPS). All peptide syntheses were based on a Fmoc strategy and were carried out manually using a modified 2-chloro-tritylchloride resin prepared as previously described.[43] The following conditions were used:

- Resin deprotection (Fmoc removal): piperidine/DMF (2/8) for 5 min, twice.
- Coupling conditions: Fmoc-AA-OH (3 equiv), HATU (3 equiv), DIEA (6 equiv), and DMF, stirred at r.t. for 30 min (double coupling (30 min) was used).
- Fmoc deprotection conditions: piperidine/DMF (2/8) at r.t. for 5 min (twice).
- Mild cleavage conditions: TFA/CH$_2$Cl$_2$ (1/99) for 5 min, four times and then MeOH/pyridine (8/2) were added, obtaining the peptide without deprotecting the amino acid side chains.
- Deprotection (Trt) and cleavage conditions: TFA/TIS/H$_2$O (95/2.5/2.5) at r.t. for 12 h and then precipitation in Et$_2$O.

The final peptides were obtained after precipitation in Et$_2$O and were all titrated by ^{1}H NMR (D$_2$O) using *tert*-butanol as the internal

reference in order to determine their exact molar concentration. For this, the compound was solubilized in D$_2$O (final concentration around 5 mM) and *tert*-butyl alcohol was added (25 μL, 13.3 mM) in an NMR tube (total volume of 600 μL). ^{1}H NMR was recorded and the relative peak integration was used to calculate the exact concentration of the compound.

UV−vis and Fluorescence Spectroscopy. UV−visible and fluorescence spectra were recorded on, respectively, UV mc^2 and FLX-Xenius XMF spectrophotometers from Safas, S.A., Monaco. The excitation wavelength was set at λ = 320 nm for fluorescence experiments.

CD Spectroscopy. CD measurements were recorded at 20 °C on a Jasco J-815 at the Laboratoire de Mesures Physiques, IBMM, Université de Montpellier.

Scanning Electronic Microscopy in Cryo Mode (Cryo-SEM). Cryo-SEM images of the organogels were obtained as following: a small piece of organogel placed onto a cryo-holder was quickly plunged into a nitrogen slush and subsequently transferred under vacuum into a Quorum PT3010 chamber attached to a microscope. The sample was then fractured with an adapted razor blade and etched at −70 °C. The sample was eventually transferred in an FEG-cryo-SEM (Hitachi SU8010) and observed at 1 kV at −150 °C.

Rheology. Rheological properties were measured on a Kinexus Malvern rheometer using a sand-blasted plate geometry of 1 cm diameter and a gap of 0.5 mm. The organogels were prepared within a homemade Teflon mold of 1 cm of diameter. The resulting materials were then removed from the mold to perform the measurements. Strain measurements were carried out from 0.01 to 100% at 0.3 Hz and frequency sweeps were performed from 0.01 to 10 Hz at a fixed strain of 0.06%.

Molecular Dynamics Simulations. Molecular dynamics (MD) simulations were performed to investigate the conformational properties of **Cage 1** and **Cage 2$_0$**. The starting conformations of both cages were built within the Avogadro molecular editor.[44] All following simulations were then achieved with the GPU version of the AMBER16 package.[45] The AM1-BCC method, as implemented in the antechamber module of AMBER16,[3] was used to calculate atomic partial charges of both cages whereas the GAFF 2.1 Force Field (FF) was employed for the other force field parameters.[46] For the torsion angle of the phenyl moieties around the central double bond of the tetraphenylethene (TPE) core, we used parameters from previous DFT calculations in order to reproduce the propeller geometry of the TPE core.[47] Molecular mechanics calculations were performed to optimize the starting geometry of the cages. For this, a steepest descent minimization of 25,000 steps was carried out, subdivided in 5000 steepest descent steps followed by 20,000 conjugate gradient steps. The MD simulations were performed for a simulation time of 5.0 μs for each cage in an implicit solvent using the Generalized Born solvation model[48] to conduct a relevant conformational sampling on the microsecond regime with reasonable computational resources. A dielectric constant of 47.2 was considered, i.e., the dielectric constant of DMSO solvent at room temperature. During the production stage, a 2 fs time step was employed as the SHAKE algorithm[49] constrained the length of covalent bonds that involved hydrogen atoms. Temperature was maintained at 300.0 K by using a Langevin thermostat with a 1.0 ps^{-1} collision frequency. MD snapshots were recorded each 1.0 ns, resulting in a 5000 frames trajectory at the end of the production MD. Analysis of the MD trajectories and extraction of the MD snapshots were performed with the CPPTRAJ module of AmberTools16. Radius of gyration (R_g) was calculated by considering the heavy atoms, with omissions of hydrogen atoms. The root-mean-square deviations (RMSDs) were calculated according to the heavy atoms of the starting conformations of the production stage. For rendering of MD snapshots, we used PyMOL 2.2.0.[50] In-house R scripts were used for statistical analyses of the raw data issued from MD trajectories.[51]

Scheme 1. General Description of the Formation of Molecular Cages and DCNs through the Hierarchical Covalent Self-Assembly of TPE-ALD with Cysteine-Rich C-Hydrazide Peptides, Which Involves Simultaneous Acyl-Hydrazone and Disulfide Bond Formation
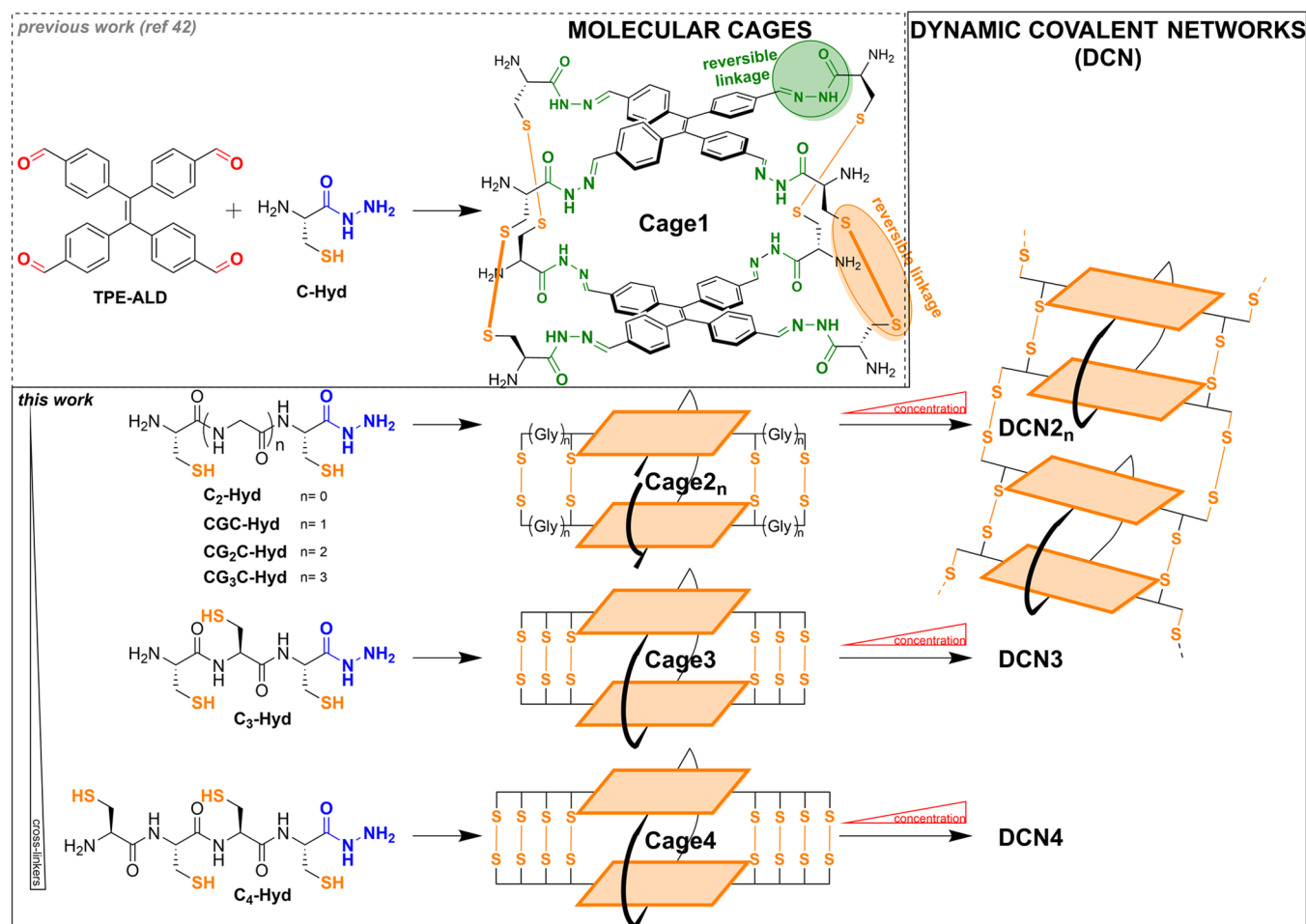
RESULTS AND DISCUSSION

Design and Synthesis. Our design rests on the use of a TPE core, which is well known to display aggregation-induced emission (AIE).[52,53] AIE was coined in 2001[54] and has since then attracted a tremendous attention for various applications in material sciences, biosensing, and bioimaging.[55−58] With most common fluorophores, aggregation causes quenching of fluorescence emission in a process called aggregation-caused quenching (ACQ). Instead, AIE fluorophores undergo restriction of intramolecular motions upon aggregation which results in a strong enhancement of their fluorescence emission.[52,53,57,59] While the propeller-like structure of TPE prevents aggregation by π−π stacking interactions, some solid-state structures have revealed partially ordered columnar aggregation mediated by CH−π interactions with some offset phenyl rings in close proximity,[60−62] and the existence of polymorphic organization make these systems mechanosensitive.[63] TPE has already been inserted in discrete cage compounds,[64−69] as well as in supramolecular polymers[70] and gels.[71,72] Stang and co-workers have recently pushed this topic one step further by elaborating a hierarchical system combining coordination and host−guest interactions that resulted in supramolecular polymer gels.[73]

Herein, we selected **TPE-ALD** (Scheme 1) as the aromatic core, which is able to reversibly react up to four times with complementary hydrazides derived from modified peptides. Indeed, we have previously shown that using C-hydrazide L-cysteine (**C-Hyd**, Scheme 1) affords, in a one-pot process involving eight acyl-hydrazone bond and four disulfide bond formation, fluorescent dynamic covalent cages.[42] Interestingly, these modified peptides can be engineered to tune solubility[74] or possibly to introduce functional groups. To go beyond molecular cages and move upward in a bottom-up manner toward materials, we hypothesized that using modified peptides with multiple L-cysteine residues would enable the dynamic cross-linking of cages, eventually leading to the formation of dynamic covalent polymer networks. This strategy has been previously implemented in the hierarchical self-assembly of peptide amphiphiles.[75−77] Of course, the key aspect is to favor inter- versus intramolecular cross-links. In this work, we selected six C-hydrazide peptides bearing multiple (2−4) L-cysteine residues (Scheme 1). These peptides were synthesized by SPPS using a modified 2-chloro-trityl chloride resin (see the Supporting Information).[43] A mild acidic cleavage (1% TFA in CH₂Cl₂) afforded the protected peptides, which were nicely purified by preparative reverse-phase HPLC and fully characterized (¹H, ¹³C NMR, and MS), before undergoing a final deprotection (TFA/TIS/H₂O 95/2.5/2.5) to yield to the final desired peptides.
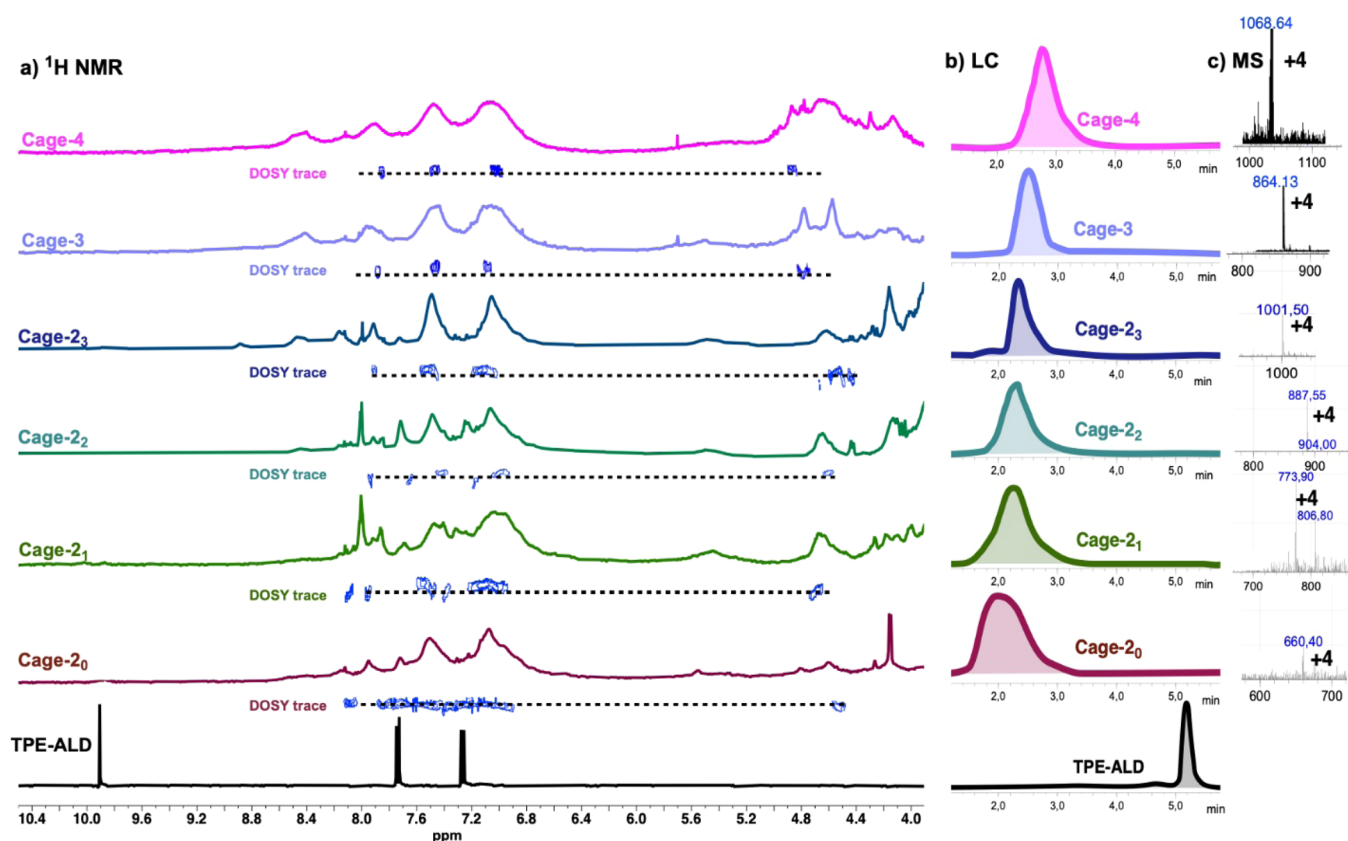
Figure 1. Formation of molecular cages by hierarchical covalent self-assembly. (a) ^{1}H NMR (600 MHz, DMSO-d$_6$) of reactions mixtures with, below, the extracted DOSY NMR spectrum; (b) HPLC chromatograms; and (c) extracted mass spectra.

Dynamic Self-Assembly of Cages. Concentration was previously found to play a major role in the outcome of the covalent self-assembly, with cage compounds typically formed at millimolar concentrations.[42] Thus, we carried out the self-assembly as previously mentioned at 2 mM in a mixture DMSO/H$_2$O (94/6, v/v) at 50 °C for 5 days, by mixing stoichiometric amounts of both building blocks.

^{1}H NMR analyses in DMSO-d$_6$ show the complete disappearance of the aldehyde peak of **TPE-ALD** (9.89 ppm) and the formation of a set of broad signals (Figure 1A). HPLC confirms the complete conversion and show a single new peak being formed (Figure 1B). DOSY NMR also indicate a single species, therefore pointing out to a mixture of isomers in equilibrium for explaining the complexity seen in ^{1}H NMR spectra (Figure 1A). Calculation of the hydrodynamic diameters using the Stokes−Einstein relationship gives values ranging from 22 to 59 Å (Table 1).

This is significantly higher than the tetra-functionalized TPE derivatives shown in Figure 2: **TPE-Ac** (19 Å hydrodynamic diameter) and **TPE-Ox** (13 Å hydrodynamic diameter). The trend shows, as expected, that longer peptide hydrazides lead to larger species of increased hydrodynamic diameters. Finally, mass spectrometry analyses reveal that the multicomponent cages are formed in all cases (Figure 1C).

Monitoring the process by fluorescence spectroscopy shows a gradual increase in the emission of TPE at 510 nm over the course of the reaction (Figure S27). In the end, after 5 days of reaction, the fluorescence emission is markedly increased by 64- to 117-fold compared to **TPE-ALD** (Figure 3A). This observation is in line with our proposed formation of cage structures where two TPE units are constrained in close

Table 1. Table of Hydrodynamic Diameters, Calculated from the DOSY Experiments Using the Stokes−Einstein Equation

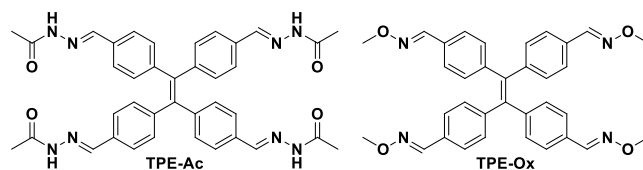| compound	D [m^2 s^{-1}]	D$_{hyd}$ [Å]
TPE-Ac	1.17×10^{-10}	18.8
TPE-Ox	1.62×10^{-10}	13.4
Cage1	9.59×10^{-11}	22.8
Cage2$_0$	5.75×10^{-11}	38.0
Cage2$_1$	6.56×10^{-11}	34.4
Cage2$_2$	6.21×10^{-11}	35.2
Cage2$_3$	4.84×10^{-11}	45.2
Cage3	4.89×10^{-11}	45.0
Cage4	3.72×10^{-11}	58.8

Figure 2. Chemical structures of **TPE-Ac** and **TPE-Ox**.

proximity, thereby promoting AIE by restriction of intramolecular motions. For comparison, **Cage1** exhibited a 61-fold increase in fluorescence emission,[42] thus suggesting that the further enhancement shown by **Cage3** and **Cage4** is due to more constraints imposed on the two TPE units by the multiple intramolecular disulfide linkages.

UV−visible absorption spectroscopy shows similar profiles for all cage compounds. Compared to the starting **TPE-ALD**,
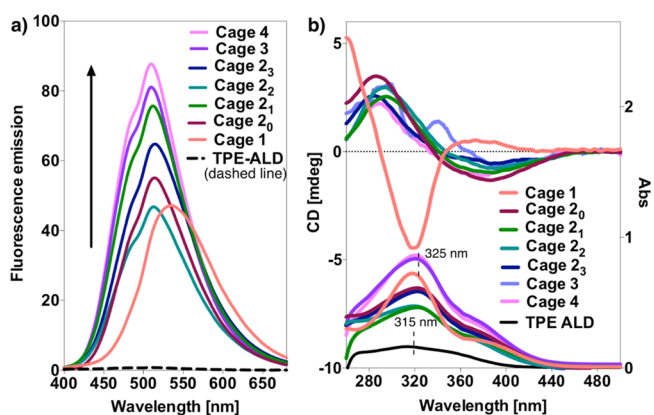
Figure 3. (a) Fluorescence and (b) UV–visible and CD spectra of cages self-assembled from **TPE-ALD** and different cysteine-rich C-hydrazide peptides. Conc. = 0.008 mM in DMSO/H$_2$O (94/6 v/v).

they display hyperchromism, a 10 nm bathochromic shift in the TPE-centered band at 315 nm, and an increasing band around 370 nm assigned to the extension of the π-electron system with the formation of the acyl-hydrazone linkages (Figure 3B). Circular dichroism (CD) studies reveal bisignate CD signals in the spectral region of TPEs, which indicate a preferred chiral organization of the TPE chromophores enforced by the chirality of the hydrazide side chains (Figure 3B). Since similar signals are observed on tetraconjugates not adopting a cage structure—with mirror-image CD spectra obtained when using enantiomeric peptides (Figure S26)—we infer that the CD signature here is induced by chiral information being transferred from the peptide side chains onto the propeller arrangement of the TPE core, rather than by an exciton coupling between the two TPE cores. Therefore, the marked difference in the CD signature between **Cage 1** and **Cage 2$_0$** (Figure 3b) is best explained by the chirality of the propeller TPE being differently affected by the two peptide side chains adopting different conformations.[78] This is also in line with fluorescence emission being blue-shifted in **Cage 1**, compared to **Cage 2$_0$**, which is indicative of a more twisted and rigid arrangement of the TPE core.[63] The CD spectrum of **Cage 1** is reminiscent of previous TPE conjugated to a single

amino acid,[79,80] whereas the CD spectrum of **Cage 2$_0$** is more similar to previous TPE conjugated to two amino acids self-organizing into chiral helical stacks in the solid state,[81,82] these cases exemplify how the nature of peptide side-groups can impact CD spectra of TPE–peptide conjugates.

MD simulations were performed to provide insights into the structures and dynamics of **Cage 1** and **Cage 2$_0$** (see Materials and Methods for computational details). The final MD snapshots of both cages is shown in Figure 4. The global size of the cages is well preserved throughout the MD time (Figure S28), with average radii of gyration of 8.7 and 10.3 Å for **Cage 1** and **Cage 2$_0$**, respectively. Regarding the conformational dynamics of the cages, the RMSD profiles are different according to the parts of the cages, i.e., the TPE cores versus the peptide chains (Figure S29). For the TPE cores, the RMSD fluctuations are very weak, although small RMSD jumps were observed, due to the fast rotation of specific phenyl moieties (see the torsion angles of phenyls around the TPE central double bond in Figures S30 and S31). Despite their rigidity, the mutual orientation between the two TPE cores is dynamic in both cages. Hence, whereas the distance between the two central double bonds is rather conserved, the angle between the central double bonds of the two TPE units is highly dynamic, with a two-peak distributions and important oscillations (Figure S32). The two rigid TPE cores can thus be positioned in different ways thanks to their twisting motions made possible by the dynamics of the flexible peptide chains. Important conformational fluctuations were indeed observed in the RMSD profiles of the peptide chains, clearly in contrast with the rigidity of the TPE cores (Figure S29). The dihedral angles along the peptide chains are dynamic and adopt a wide variety of Ψ torsion angles (see the multipeak distribution in Figures S33 and S34). Importantly, we observed a shift in the distributions of most of the Ψ torsion angles that are proximal to the TPE cores when going from **Cage 1** to **Cage 2$_0$**. As an example, we report in Figure 4 the distribution of one Ψ dihedral angle close to the TPE core for **Cage 1** and **Cage 2$_0$**. MD simulations revealed an increase of the planarity near the TPE core for **Cage 2$_0$**, compared to **Cage 1**. This difference of dihedral angles near the TPE cores for the two cages could explain the large differences in their CD spectra. Similarly, the dihedral angles around the disulfide
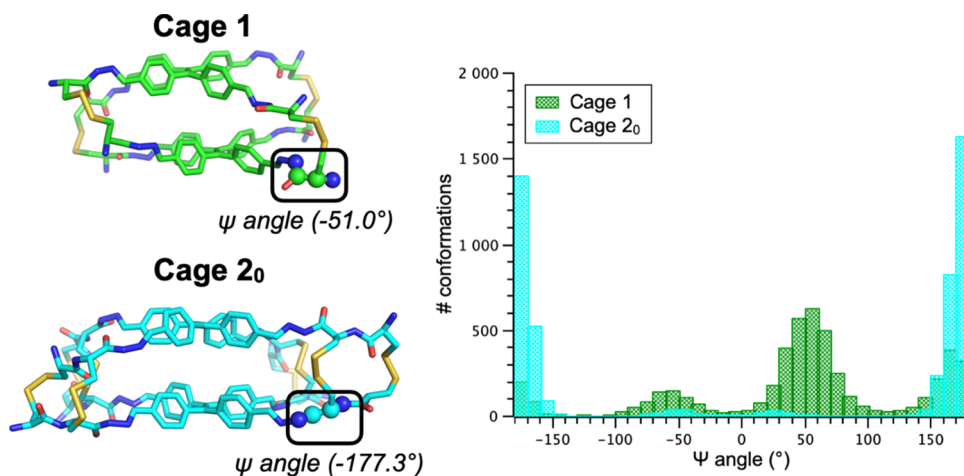

Figure 4. Side view of the final MD snapshots of **Cage 1** and **Cage 2$_0$**. Hydrogen atoms were omitted for clarity. The atoms represented in spheres are related to a specific Ψ dihedral angle for which the distributions issued from the MD simulations are shown on the right. **Cage 2$_0$** has more extended arms with the planarization of the Ψ dihedral angle compared to **Cage 1**.

bonds are also impacted, showing different distributions for both cages (Figures S35 and S36).

Since these cage compounds feature two reversible covalent linkages, they may respond to two different chemical stimuli.[83] We previously explored the effect of methoxyamine, which enforced covalent exchange of the acyl-hydrazones, leading to a controlled dissociation of the cage.[42] Here, by monitoring the fluorescence emission, we confirm that all new cages degrade ($t_{1/2} \approx 3-12$ h) in the presence of methoxyamine (20 equiv), leading, as previously demonstrated,[42] to the formation of **TPE-Ox** (Figure S37). CD spectroscopy shows the disappearance of the bisignate signals, as the chiral cages are transformed into the achiral **TPE-Ox** in the process (Figure S38). Additionally, we tested the dissociation of the new cages in the presence of the reducing agent β-mercaptoethanol (BME) (100 equiv). Fluorescence studies show degradation of the cage compounds albeit at a lower rate ($t_{1/2} \approx 12-24$ h) than during the methoxyamine-promoted degradation (Figure S37). In this case, CD spectra show a weakening of the signals with, nevertheless, a nonzero final signal arising from acyl-hydrazone tetrafunctionalized chiral conjugates of TPE bearing different peptides being generated (Figure S38).

Dynamic Self-Assembly of Dynamic Covalent Polymer Networks. Since intermolecular associations are favored at concentrations above the effective molarity, amplifying chains at the expense of rings,[84] we studied the outcome of the covalent self-assembly at increasing concentrations of **TPE-ALD** (from 10 to 100 mM in DMSO), keeping the same stoichiometric amount of peptide hydrazides and the same reaction conditions (50 °C).

DOSY NMR shows a sharp increase in the hydrodynamic diameter with the concentration (Figures 5 and S25). Since
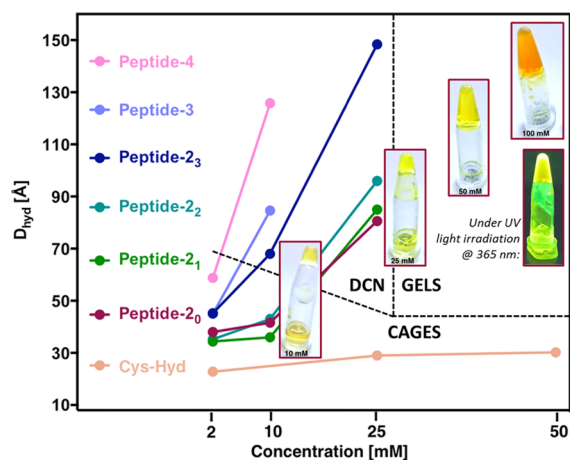
Figure 5. Observed evolution of hydrodynamic diameters, calculated from the diffusion coefficient measured by DOSY NMR using the Einstein–Stokes equation, as a function of the concentration of **TPE-ALD** in DMSO-d_6 reacting with the different cysteine-rich C-hydrazide peptides. The photographs in insets represent the representative reaction mixture with **C$_2$-Hyd** showing a flowing solution at 10 and 25 mM and a self-standing gel at 50 and 100 mM.

Cage1, which is unable to form DCNs because it contains a single thiol, did not display such increase in the hydrodynamic diameter, we concluded that this observed increase in the hydrodynamic diameter is not simply the result of supramolecular aggregation but rather the consequence of the formation of DCNs, which is promoted by intermolecular

disulfide cross-links. In further support of this conclusion, we interestingly observed in all cases, the formation of fluorescent gels at high concentrations where, in contrast, **Cage1** remains a solution (Figure 5). Thus, we found the critical gelation concentration to go with the number of cysteines present within the peptide building blocks. Whereas gels were visually observed at concentrations above 50 mM with peptides **C$_2$-Hyd**, **CGC-Hyd**, **CG$_2$C-Hyd**, and **CG$_3$C-Hyd**, which all contain two cysteine residues, gels were already observed at 25 mM with peptides **C$_3$-Hyd** and **C$_4$-Hyd**, which display, respectively, three and four cysteine residues. These results are in line with the Carothers theory, which predicts that the gel point decreases with increasing functionality of monomers.[85]

Visually, all gels were also found to be brightly fluorescent upon light irradiation at 365 nm (see the inset photograph in Figure 5). Spectroscopic analyses of the DCN solutions revealed a stronger AIE effect of the DCN compared to the cages, with fluorescence emissions now increased by 103- to 133-fold compared to **TPE-ALD** (Figure 6A). UV–visible absorption shows comparable spectra, while CD spectra show similar but more intense signatures that indicate a more predominant chiral environment (Figure 6B).
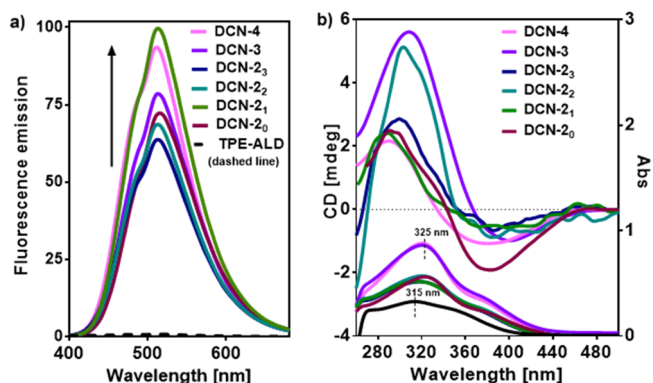
Figure 6. (a) Normalized fluorescence spectra and (b) CD/UV–vis studies for DCNs (94/6 DMSO/H$_2$O v/v). Conc. = 0.008 mM.

In addition to the two dynamics endowed by the acyl-hydrazone and disulfide reversible covalent linkages (vide infra), these DCNs are also sensitive to concentration—lowering concentration is expected to trigger the conversion from DCNs to cage compounds—which we considered in the following study of the controlled degradation of these DCNs. Since fluorescence emission is a marker of the formation of DCNs, their degradation was monitored by fluorescence spectroscopy. Generally speaking, all DCNs showed the same trends (Figure 7). Concentration has a slow and weak effect on the fluorescence emission (emission dropping about 10–40% with $t_{1/2} \approx 5-20$ h), which is compatible with a conversion of the DCN back into the cage compounds. The addition of BME (100 equiv) has a slow but a complete effect quenching the fluorescence emission down to the level of **TPE-ALD**. We interpret this as the breakage of the DCN by the reduction of disulfide cross-links, and the formation of TPE tetraacylhydrazone conjugates. On the other hand, the addition of methoxyamine (20 equiv) has a more rapid effect with a complete quenching of the AIE, which is explained by the ultimate formation of **TPE-Ox**. These interpretations are supported by CD studies, which show a gradual decrease of the Cotton effect upon treatment with BME, and a complete
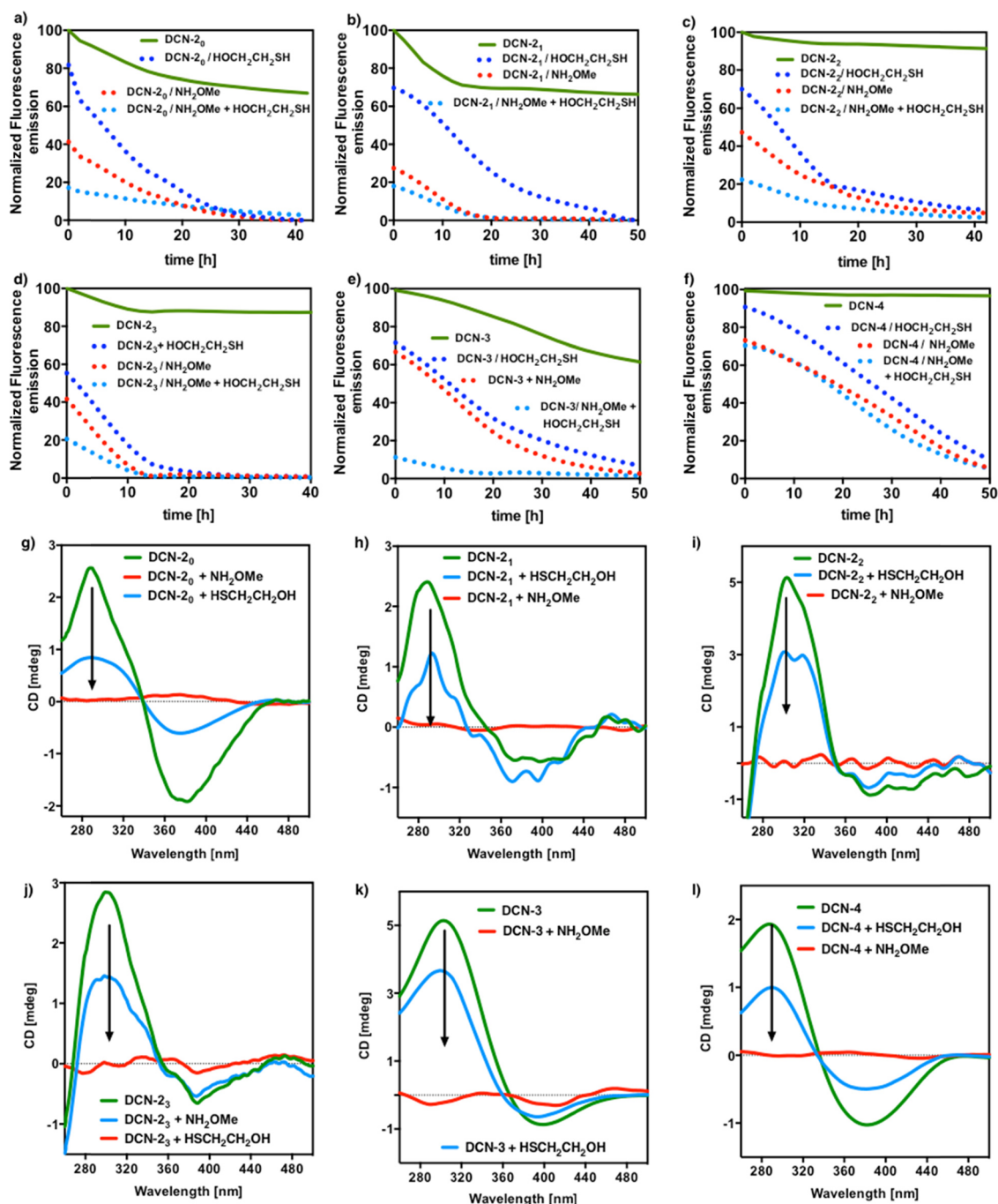
Figure 7. Chemically controlled degradation of DCNs, made from different cysteine-rich C-hydrazide peptides, monitored by fluorescence (a−f) and CD (g−l) spectroscopies upon addition of methoxyamine (20 equiv) and/or β-mercaptoethanol (100 equiv) in 94/6 DMSO/H$_2$O v/v. [DCN] = 0.008 mM for fluorescence and 0.02 mM for CD measurements. The fluorescence emission values are normalized to the initial and highest value. CD spectra were recorded ca. 1 min after the addition of the chemical cues with HT$_{max}$ < 450 V.

suppression when methoxyamine was added (Figure 7). While the persisting Cotton effect in the former case is explained by the presence of chiral TPE acyl-hydrazone conjugates, the formation of the achiral **TPE-Ox** explains the absence of CD signals in the TPE absorption region. Interestingly, these marked changes observed by CD are seen at short reaction times, down to 1 min, thereby indicating that important structural changes occur rapidly within the DCNs at this 2.5× higher concentration of 20 μM. Finally, the combination of both stimuli actually shows a weak synergistic action in the degradation of the DCN, which now takes place with $t_{1/2}$ < 5 h

expect for **DCN4**, which is the most stable. This is best explained by the proposal that fast breakage of the acyl-hydrazone covalent bonds induced local loss of the structure, which facilitates diffusion of BME in order to break disulfide linkages.

The chemically triggered degradation of **DCN2** was also observed visually on the gels obtained at 50 mM. Physical degradation was observed upon addition a drop of methoxyamine or BME in 94/6 DMSO/H$_2$O, whereas addition of the solvent alone did not have the same effect on this time scale (Figure 8).
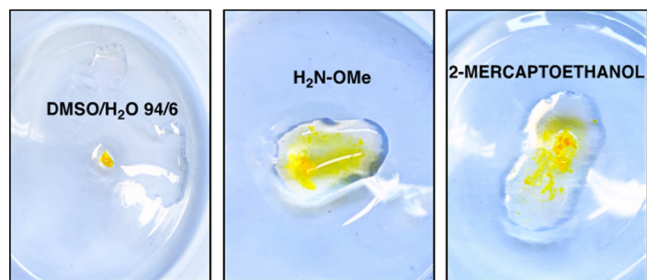
Figure 8. Chemically triggered degradation of the **DCN2** gel, obtained from the hierarchical covalent self-assembly performed at 50 mM, upon addition of methoxyamine (middle) or β-mercaptoethanol (right) in 94/6 DMSO/H$_2$O v/v. Control experiments with addition of solvent alone is shown on the left panel. Photographs were taken 15 min after incubation at room temperature.

Since disulfides are capable of photoinduced radical disulfide metathesis under UV light irradiation,[22] we irradiated our DCNs with a laboratory lamp (6 W) at either 254 or 365 nm. The results show, with both wavelengths and for all DCNs, a remarkable degradation of the DCN with $t_{1/2} \approx 3-5$ h (Figure 9). This is in stark contrast with the behavior of the cage compounds, which remain essentially unaffected during light irradiation, as monitored by fluorescence spectroscopy and LC−MS (Figure S39). Our proposed interpretation is that light irradiation triggers photoinduced radical disulfide meta-

thesis of the least stable intercage disulfide connectors, which then rearrange intramolecularly to produce single TPE conjugates that display low fluorescence emission. Thus, it seems that the degradation of the DCNs under light irradiation takes a different pathway, compared to their rearrangement in diluted conditions, forming single TPE conjugates rather than cage compounds.

Rheological Analyses. The mechanical properties of all the following DCN gels, **DCN2$_0$**, **DCN2$_1$**, **DCN2$_2$**, **DCN2$_3$**, and **DCN3** were determined by dynamic oscillatory rheology providing information about the storage (G′) and the loss moduli (G″). These materials were prepared from 50 mM **TPE-ALD** in DMSO, as mentioned previously. G′ (i.e., storage modulus) is an indicator of the elastic behavior of the material by measuring its ability to store deformation energy, which can be recovered after removing the applied load. G″ (i.e., loss modulus) measures the deformation energy that is dissipated as heat and friction during the shearing process. Strain sweep tests were carried out to determine the linear viscoelastic region, defined as the region where the G′ and G″ are parallel and independent of the strain amplitude. All measurements are given in Figure S40 and show that the G′ values are higher than the G″ values (G′ > G″) in the frequency range studied, in all cases. This confirms the gel-like behavior for all DCNs. In addition, we also notice that the G″ value does not vary with the increase in strain, a behavior in agreement with a covalently
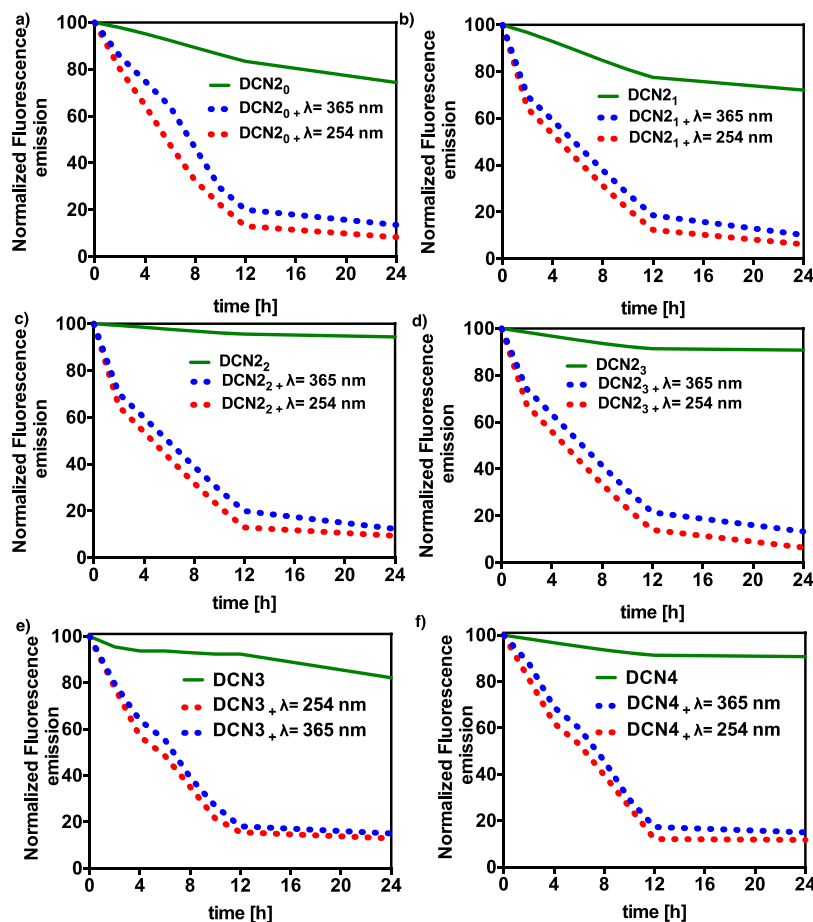

Figure 9. Light-triggered degradation of DCNs, made from different cysteine-rich C-hydrazide peptides (a) **DCN2$_0$**, (b) **DCN2$_1$**, (c) **DCN2$_2$**, (d) **DCN2$_3$**, (e) **DCN3**, and (f) **DCN4**, monitored by fluorescence spectroscopy upon irradiation for 24 h under UV light (λ = 254 and λ = 365 nm) of solutions of DCNs (0.008 mM) in 94/6 DMSO/H$_2$O v/v. The fluorescence emission values are normalized to the initial and highest value.
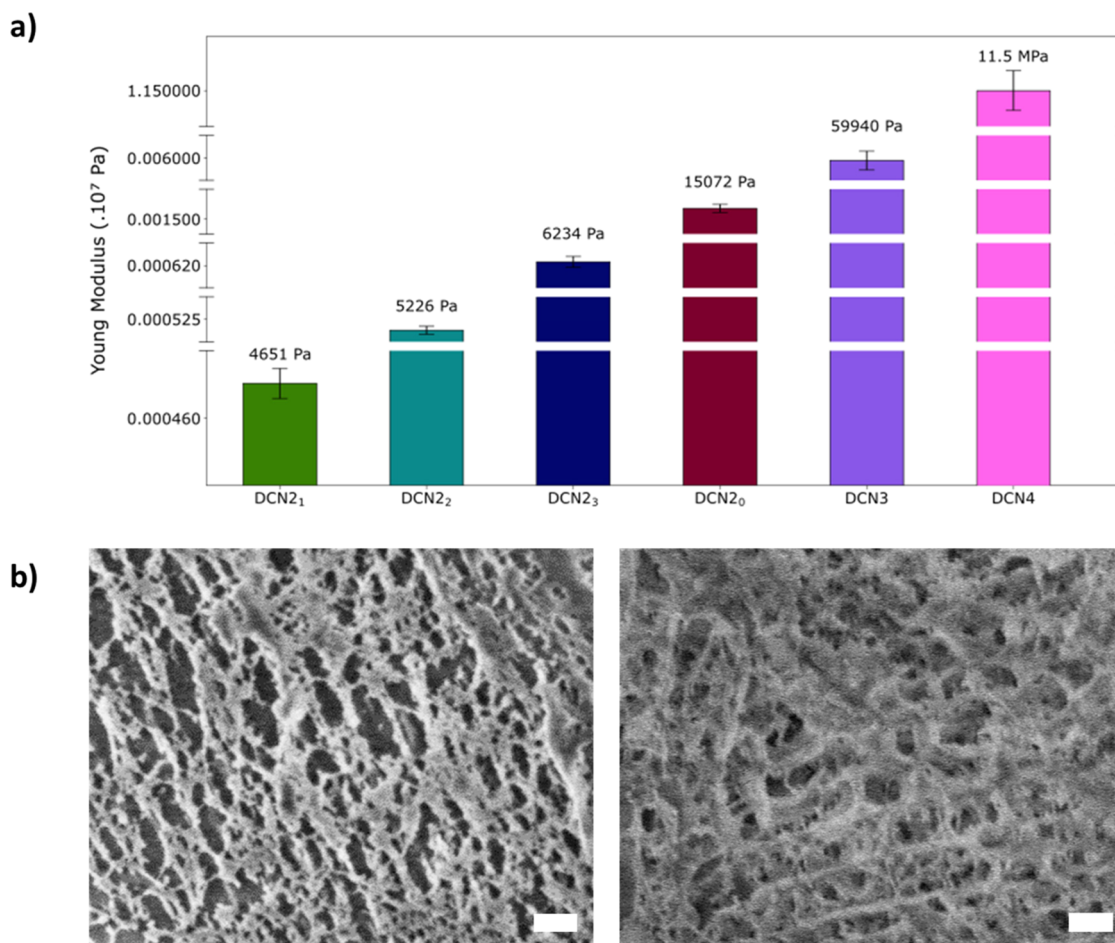
Figure 10. (a) Histogram of the Young modulus E of the following gels: $DCN2_0$, $DCN2_1$, $DCN2_2$, $DCN2_3$, **DCN3**, and **DCN4** determined by dynamic oscillatory rheology using a frequency sweep of 1 Hz, except for **DCN4** for which E was determined from nanoindentation measurements. The mean values and their standard deviation have been determined from two independent measurements for $DCN2_0$, $DCN2_1$, $DCN2_2$, $DCN2_3$, and DCN_3, and four independent measurements for DCN_4. (b) Typical cryo-SEM images of $DCN2_0$ (left) and $DCN2_1$ (right) gels. The white scale bar indicates 200 nm.

cross-linking material. Despite the 5 days implemented to get a mechanically robust organogel that pass the inversion test tube (Figure 5), gel point monitoring shows that the liquid–gel transition occurs more rapidly: for instance, this transition is observed when G′ and G″ curves intersect overtime, roughly 22 min after mixing **TPE-ALD** and **C2-Hyd** together at 50 mM and 50 °C, leading to $DCN2_0$ (Figure S41). In first approximation, the Young modulus E, also called modulus of elasticity, can be estimated as three times the value of G′. Thus, E values of $DCN2_0$, $DCN2_1$, $DCN2_2$, $DCN2_3$, and **DCN3** gels are given in Figure 10a. When **C4-Hyd** is used, the **DCN4** gel obtained is so stiff that the dynamic oscillatory rheology approach is not adapted to measure its Young modulus E. Indeed, the resulting **DCN4** gel has a macroscopic glasslike behavior and nanoindentation was required to characterize its mechanical properties. An E value of 11.5 MPa is measured for the **DCN4** gel (Figure S42). The E value slightly increases from $DCN2_1$, $DCN2_2$ to $DCN2_3$, going from 4.6, 5.2 to 6.2 kPa, respectively. In these three gels, the number of cysteine residues is two, only the degree of freedom between them is increasing through the number of glycine residues between them. This slight linear increase of E going from $DCN2_1$, $DCN2_2$ to $DCN2_3$ can be due to a better ability to form disulfide bridges when a higher number of glycine spacers

are used. However, in the case of the $DCN2_0$ gel, the E value is roughly three times higher than for $DCN2_1$, $DCN2_2$ to $DCN2_3$, to reach 15.1 kPa. In this case, the absence of a spacer between the two cysteine residues of C_2-**Hyd** seems related to the higher stiffness observed. When the number of cysteine residues is increased, using **C3-Hyd** and **C4-Hyd** to get the corresponding **DCN3** and **DCN4** gels, the evolution of the E value increases exponentially since values of 59.7 kPa and 11.5 MPa were measured, respectively, for these two gels. This result highlights the huge and direct relation between the number of possible covalent cross-linking points and the resulting mechanical properties of the organogels formed.

Gel state results from an internal architecture allowing the entrapping of the solvent, i.e., DMSO. The characterization of this organization can be realized by cryo-SEM. We thus have tried to get cryo-SEM images from all $DCN2_0$, $DCN2_1$, $DCN2_2$, $DCN2_3$, **DCN3**, and **DCN4** gels but we only succeeded to get suitable images for $DCN2_0$ and $DCN2_1$ gels (Figure 10b). It must be noted that the analysis of DMSO-based organogels through this approach is a challenging task because of the difficulty to sublime DMSO and concomitantly keep the organic architecture. For $DCN2_0$ and $DCN2_1$ gels, a dense nanofibrous network is observed. Thinner fibers having roughly 24 nm diameter have been measured in case of

DCN2$_0$ (Figure S43), but association of them to form larger microfibrils are mainly present in the whole material.

CONCLUSIONS

We reported herein the one-pot hierarchical self-assembly of multicomponent fluorescent DCNs through the simultaneous combination of disulfide and acyl-hydrazone bond formation. We characterized and discussed in details the outcome of the covalent self-assembly process, yielding cage compounds at concentrations of 2 mM, soluble fluorescent DCNs, and even chemically cross-linked fluorescent organogels at higher concentrations. The increase of cysteine residues in the peptide sequence from two, three to four has a huge effect on the resulting Young's modulus of the organogel formed, going from roughly 5 kPa to 1.15 MPa. For the softer gels, the internal architecture is ensured by a nanofibrillar network. Thinner fibers display a 24 nm diameter and are long over several hundred micrometers. These materials display multi-dynamic responsiveness following concentration changes, two chemical triggers, as well as light irradiation, all of which enable their controlled degradation with concomitant changes in spectroscopic (fluorescence and CD) outputs. Given the adaptive structure−function relationships of these DCNs, a future direction of investigation will be to explore their potential in bioapplications (capitalizing on a disassembly of the DCNs promoted by intracellular glutathione) or in sensing (for instance the organization and fluorescence output may respond to mechanical stress[86−88]) applications. Finally, the simplicity of our one-pot procedure that rely on a covalent self-assembly without external reagents or catalysts and the straightforward possibility to append additional functional groups at the N-terminus of the peptide building blocks[74] are strong advantages for future investigations toward smart stimuli-responsive soft materials.

ASSOCIATED CONTENT

ⓢ Supporting Information

The Supporting Information is available free of charge at https://pubs.acs.org/doi/10.1021/acs.biomac.1c01389.

> ^{1}H and ^{13}C NMR, HPLC, and mass spectrometry characterization data of all peptides, DOSY NMR of DCNs, CD analyses of enantiomeric cages, kinetic monitoring of cage formation by fluorescence spectroscopy, molecular modeling data, chemically triggered degradation of cages, photosensitivity of cage compounds, and mechanical characterization (PDF)

AUTHOR INFORMATION

Corresponding Authors

Mathieu Surin − *Laboratory for Chemistry of Novel Materials, Center of Innovation and Research in Materials and Polymers, University of Mons-UMONS, 7000 Mons, Belgium;* ⓞ orcid.org/0000-0001-8950-3437; Email: mathieu.surin@umons.ac.be

Loïc Jierry − *Université de StrasbourgCNRS, Institut Charles Sadron, 67034 Strasbourg, France;* Email: ljierry@unistra.fr

Sébastien Ulrich − *Institut des Biomolécules Max Mousseron (IBMM), CNRS, Université of Montpellier, ENSCM, 34090 Montpellier, France;* ⓞ orcid.org/0000-0002-6080-3345; Email: sebastien.ulrich@cnrs.fr

Authors

Esteban Suárez-Picado − *Institut des Biomolécules Max Mousseron (IBMM), CNRS, Université of Montpellier, ENSCM, 34090 Montpellier, France;* Present Address: Centro de Investigacións Científicas Avanzadas (CICA), Universidade da Coruña, 15071 A Coruña, Spain; ⓞ orcid.org/0000-0003-1161-8175

Maëva Coste − *Institut des Biomolécules Max Mousseron (IBMM), CNRS, Université of Montpellier, ENSCM, 34090 Montpellier, France*

Jean-Yves Runser − *Université de StrasbourgCNRS, Institut Charles Sadron, 67034 Strasbourg, France*

Mathieu Fossépré − *Laboratory for Chemistry of Novel Materials, Center of Innovation and Research in Materials and Polymers, University of Mons-UMONS, 7000 Mons, Belgium*

Alain Carvalho − *Université de StrasbourgCNRS, Institut Charles Sadron, 67034 Strasbourg, France*

Complete contact information is available at:
https://pubs.acs.org/10.1021/acs.biomac.1c01389

Author Contributions

The manuscript was written through contributions of all authors. All authors have given approval to the final version of the manuscript.

Notes

The authors declare no competing financial interest.

ACKNOWLEDGMENTS

REFERENCES

(1) Zhang, W.; Jin, Y., *Dynamic Covalent Chemistry: Principles, Reactions, and Applications*; Wiley-VCH: Weinheim, 2017.

(2) Rowan, S. J.; Cantrill, S. J.; Cousins, G. R. L.; Sanders, J. K. M.; Stoddart, J. F. Dynamic covalent chemistry. *Angew. Chem., Int. Ed.* **2002**, *41*, 898−952.

(3) Jin, Y. H.; Wang, Q.; Taynton, P.; Zhang, W. Dynamic Covalent Chemistry Approaches Toward Macrocycles, Molecular Cages, and Polymers. *Acc. Chem. Res.* **2014**, *47*, 1575−1586.

(4) Zhang, Y.; Qi, Y.; Ulrich, S.; Barboiu, M.; Ramström, O. Dynamic covalent polymers for biomedical applications. *Mater. Chem. Front.* **2020**, *4*, 489−506.

(5) Chakma, P.; Konkolewicz, D. Dynamic Covalent Bonds in Polymeric Materials. *Angew. Chem., Int. Ed.* **2019**, *58*, 9682−9695.

(6) Garcia, F.; Smulders, M. M. J. Dynamic Covalent Polymers. *J. Polym. Sci., Part A: Polym. Chem.* **2016**, *54*, 3551−3577.

(7) Roy, N.; Bruchmann, B.; Lehn, J. M. DYNAMERS: dynamic polymers as self-healing materials. *Chem. Soc. Rev.* **2015**, *44*, 3786−3807.

(8) Lehn, J.-M. Dynamers: dynamic molecular and supramolecular polymers. *Progr. Polym. Sci.* **2005**, *30*, 814−831.

(9) Zheng, N.; Xu, Y.; Zhao, Q.; Xie, T. Dynamic Covalent Polymer Networks: A Molecular Platform for Designing Functions beyond

Chemical Recycling and Self-Healing. *Chem. Rev.* **2021**, *121*, 1716−1745.

(10) Wemyss, A. M.; Ellingford, C.; Morishita, Y.; Bowen, C.; Wan, C. Dynamic Polymer Networks: A New Avenue towards Sustainable and Advanced Soft Machines. *Angew. Chem., Int. Ed.* **2021**, *60*, 13725−13736.

(11) Wojtecki, R. J.; Meador, M. A.; Rowan, S. J. Using the dynamic bond to access macroscopically responsive structurally dynamic polymers. *Nat. Mater.* **2011**, *10*, 14−27.

(12) Li, X. Q.; Stepanenko, V.; Chen, Z. J.; Prins, P.; Siebbeles, L. D. A.; Wurthner, F. Functional organogels from highly efficient organogelator based on perylene bisimide semiconductor. *Chem. Commun.* **2006**, *37*, 3871−3873.

(13) Dawn, A.; Shiraki, T.; Haraguchi, S.; Tamaru, S.; Shinkai, S. What Kind of "Soft Materials" Can We Design from Molecular Gels? *Chem. − Asian J.* **2011**, *6*, 266−282.

(14) Chao, A.; Negulescu, J.; Zhang, D. H. Dynamic Covalent Polymer Networks Based on Degenerative Imine Bond Exchange: Tuning the Malleability and Self-Healing Properties by Solvent. *Macromolecules* **2016**, *49*, 6277−6284.

(15) Boekhoven, J.; Poolman, J. M.; Maity, C.; Li, F.; van der Mee, L.; Minkenberg, C. B.; Mendes, E.; van Esch, J. H.; Eelkema, R. Catalytic control over supramolecular gel formation. *Nat. Chem.* **2013**, *5*, 433−437.

(16) Trausel, F.; Versluis, F.; Maity, C.; Poolman, J. M.; Lovrak, M.; van Esch, J. H.; Eelkema, R. Catalysis of Supramolecular Hydrogelation. *Acc. Chem. Res.* **2016**, *49*, 1440−1447.

(17) Chu, C. W.; Stricker, L.; Kirse, T. M.; Hayduk, M.; Ravoo, B. J. Light-Responsive Arylazopyrazole Gelators: From Organic to Aqueous Media and from Supramolecular to Dynamic Covalent Chemistry. *Chem. − Eur. J.* **2019**, *25*, 6131−6140.

(18) Zhang, X. Y.; Waymouth, R. M. 1,2-Dithiolane-Derived Dynamic, Covalent Materials: Cooperative Self-Assembly and Reversible Cross-Linking. *J. Am. Chem. Soc.* **2017**, *139*, 3822−3833.

(19) Barcan, G. A.; Zhang, X. Y.; Waymouth, R. M. Structurally Dynamic Hydrogels Derived from 1,2-Dithiolanes. *J. Am. Chem. Soc.* **2015**, *137*, 5650−5653.

(20) Huang, S.; Kong, X.; Xiong, Y. S.; Zhang, X. R.; Chen, H.; Jiang, W. Q.; Niu, Y. Z.; Xu, W. L.; Ren, C. G. An overview of dynamic covalent bonds in polymer material and their applications. *Eur. Polym. J.* **2020**, *141*, No. 110094.

(21) Li, J. W.; Carnall, J. M. A.; Stuart, M. C. A.; Otto, S. Hydrogel Formation upon Photoinduced Covalent Capture of Macrocycle Stacks from Dynamic Combinatorial Libraries. *Angew. Chem., Int. Ed.* **2011**, *50*, 8384−8386.

(22) Klepel, F.; Ravoo, B. J. Dynamic covalent chemistry in aqueous solution by photoinduced radical disulfide metathesis. *Org. Biomol. Chem.* **2017**, *15*, 3840−3842.

(23) Peeler, D. J.; Sellers, D. L.; Pun, S. H. pH-Sensitive Polymers as Dynamic Mediators of Barriers to Nucleic Acid Delivery. *Bioconjugate Chem.* **2019**, *30*, 350−365.

(24) Binauld, S.; Stenzel, M. H. Acid-degradable polymers for drug delivery: a decade of innovation. *Chem. Commun.* **2013**, *49*, 2082−2102.

(25) Meng, F. H.; Hennink, W. E.; Zhong, Z. Reduction-sensitive polymers and bioconjugates for biomedical applications. *Biomaterials* **2009**, *30*, 2180−2198.

(26) Shi, Z. Y.; Wu, J. N.; Song, Q. C.; Gostl, R.; Herrmann, A. Toward Drug Release Using Polymer Mechanochemical Disulfide Scission. *J. Am. Chem. Soc.* **2020**, *142*, 14725−14732.

(27) Huo, S.; Zhao, P.; Shi, Z.; Zou, M.; Yang, X.; Warszawik, E.; Loznik, M.; Gostl, R.; Herrmann, A. Mechanochemical bond scission for the activation of drugs. *Nat. Chem.* **2021**, *13*, 131−139.

(28) Shi, Z.; Song, Q.; Göstl, R.; Herrmann, A. Mechanochemical activation of disulfide-based multifunctional polymers for theranostic drug release. *Chem. Sci.* **2021**, *12*, 1668−1674.

(29) Fritze, U. F.; von Delius, M. Dynamic disulfide metathesis induced by ultrasound. *Chem. Commun.* **2016**, *52*, 6363−6366.

(30) Zhang, X. J.; Malhotra, S.; Molina, M.; Haag, R. Micro- and nanogels with labile crosslinks - from synthesis to biomedical applications. *Chem. Soc. Rev.* **2015**, *44*, 1948−1973.

(31) Wei, Z.; Yang, J. H.; Zhou, J. X.; Xu, F.; Zrinyi, M.; Dussault, P. H.; Osada, Y.; Chen, Y. M. Self-healing gels based on constitutional dynamic chemistry and their potential applications. *Chem. Soc. Rev.* **2014**, *43*, 8114−8131.

(32) Dahlke, J.; Zechel, S.; Hager, M. D.; Schubert, U. S. How to Design a Self-Healing Polymer: General Concepts of Dynamic Covalent Bonds and Their Application for Intrinsic Healable Materials. *Adv. Mater. Interfaces* **2018**, *5*, No. 1800051.

(33) Christensen, P. R.; Scheuermann, A. M.; Loeffler, K. E.; Helms, B. A. Closed-loop recycling of plastics enabled by dynamic covalent diketoenamine bonds. *Nat. Chem.* **2019**, *11*, 442−448.

(34) Rest, C.; Kandanelli, R.; Fernandez, G. Strategies to create hierarchical self-assembled structures via cooperative non-covalent interactions. *Chem. Soc. Rev.* **2015**, *44*, 2543−2572.

(35) Vantomme, G.; Meijer, E. W. The construction of supramolecular systems. *Science* **2019**, *363*, 1396−1397.

(36) Orrillo, A. G.; Escalante, A. M.; Martinez-Amezaga, M.; Cabezudo, I. L. E.; Furlan, R. L. E. Molecular networks in dynamic multilevel systems. *Chem. − Eur. J.* **2018**, *25*, 1118−1127.

(37) Deng, G. H.; Li, F. Y.; Yu, H. X.; Liu, F. Y.; Liu, C. Y.; Sun, W. X.; Jiang, H. F.; Chen, Y. M. Dynamic Hydrogels with an Environmental Adaptive Self-Healing Ability and Dual Responsive Sol-Gel Transitions. *ACS Macro Lett.* **2012**, *1*, 275−279.

(38) Lee, S. H.; Shin, S. R.; Lee, D. S. Self-healing of cross-linked PU via dual-dynamic covalent bonds of a Schiff base from cystine and vanillin. *Mater. Design* **2019**, *172*, No. 107774.

(39) Hammer, L.; Van Zee, N. J.; Nicolay, R. Dually Crosslinked Polymer Networks Incorporating Dynamic Covalent Bonds. *Polymer* **2021**, *13*, 396.

(40) Zhang, Y.; Wang, Q.; Wang, Z.; Zhang, D.; Gu, J.; Ye, K.; Su, D.; Zhang, Y.; Chen, J.; Barboiu, M. Strong, Self-Healing Gelatin Hydrogels Cross-Linked by Double Dynamic Covalent Chemistry. *ChemPlusChem* **2021**, *86*, 1524−1529.

(41) Collins, J.; Nadgorny, M.; Xiao, Z. Y.; Connal, L. A. Doubly Dynamic Self-Healing Materials Based on Oxime Click Chemistry and Boronic Acids. *Macromol. Rapid Commun.* **2017**, *38*, No. 1600760.

(42) Drozdz, W.; Bouillon, C.; Kotras, C.; Richeter, S.; Barboiu, M.; Clément, S.; Stefankiewicz, A. R.; Ulrich, S. Generation of Multicomponent Molecular Cages using Simultaneous Dynamic Covalent Reactions. *Chem. − Eur. J.* **2017**, *23*, 18010−18018.

(43) Bartolami, E.; Bessin, Y.; Bettache, N.; Gary-Bobo, M.; Garcia, M.; Dumy, P.; Ulrich, S. Multivalent DNA recognition by self-assembled clusters: deciphering structural effects by fragments screening and evaluation as siRNA vectors. *Org. Biomol. Chem.* **2015**, *13*, 9427−9438.

(44) Hanwell, M. D.; Curtis, D. E.; Lonie, D. C.; Vandermeersch, T.; Zurek, E.; Hutchison, G. R. Avogadro: an advanced semantic chemical editor, visualization, and analysis platform. *Aust. J. Chem.* **2012**, *4*, 17.

(45) Case, D. A.; Cheatham, T. E., 3rd; Darden, T.; Gohlke, H.; Luo, R.; Merz, K. M., Jr.; Onufriev, A.; Simmerling, C.; Wang, B.; Woods, R. J. The Amber biomolecular simulation programs. *J. Comput. Chem.* **2005**, *26*, 1668−1688.

(46) Wang, J. M.; Wolf, R. M.; Caldwell, J. W.; Kollman, P. A.; Case, D. A. Development and testing of a general amber force field. *J. Comput. Chem.* **2004**, *25*, 1157−1174.

(47) Kotras, C.; Fossépré, M.; Roger, M.; Gervais, V.; Richeter, S.; Gerbier, P.; Ulrich, S.; Surin, M.; Clément, S. A Cationic Tetraphenylethene as a Light-Up Supramolecular Probe for DNA G-Quadruplexes. *Front. Chem.* **2019**, *7*, 493.

(48) Hawkins, G. D.; Cramer, C. J.; Truhlar, D. G. Pairwise solute descreening of solute charges from a dielectric medium. *Chem. Phys. Lett.* **1995**, *246*, 122−129.

(49) Ryckaert, J.-P.; Ciccotti, G.; Berendsen, H. J. C. Numerical integration of the cartesian equations. *J. Comput. Phys.* **1977**, *23*, 327−341.

(50) The Pymol Molecular Graphics System, version 2.0; Schrödinger LLC; www.pymol.org (accessed 24th of October, 2021).

(51) R Core Team; R Foundation for Statistical Computing: Vienna, Austria, 2013; www.R-project.org (accessed 24th of October, 2021).

(52) Mei, J.; Hong, Y. N.; Lam, J. W. Y.; Qin, A. J.; Tang, Y. H.; Tang, B. Z. Aggregation-Induced Emission: The Whole Is More Brilliant than the Parts. *Adv. Mater.* **2014**, *26*, 5429−5479.

(53) Hong, Y. N.; Lam, J. W. Y.; Tang, B. Z. Aggregation-induced emission. *Chem. Soc. Rev.* **2011**, *40*, 5361−5388.

(54) Luo, J. D.; Xie, Z. L.; Lam, J. W. Y.; Cheng, L.; Chen, H. Y.; Qiu, C. F.; Kwok, H. S.; Zhan, X. W.; Liu, Y. Q.; Zhu, D. B.; Tang, B. Z. Aggregation-induced emission of 1-methyl-1,2,3,4,5-pentaphenylsilole. *Chem. Commun.* **2001**, *18*, 1740−1741.

(55) La, D. D.; Bhosale, S. V.; Jones, L. A.; Bhosale, S. V. Tetraphenylethylene-Based AIE-Active Probes for Sensing Applications. *ACS Appl. Mater. Interfaces* **2018**, *10*, 12189−12216.

(56) Zhao, Z. J.; Lam, J. W. Y.; Tang, B. Z. Tetraphenylethene: a versatile AIE building block for the construction of efficient luminescent materials for organic light-emitting diodes. *J. Mater. Chem.* **2012**, *22*, 23726−23740.

(57) Mei, J.; Leung, N. L. C.; Kwok, R. T. K.; Lam, J. W. Y.; Tang, B. Z. Aggregation-Induced Emission: Together We Shine, United We Soar! *Chem. Rev.* **2015**, *115*, 11718−11940.

(58) Kwok, R. T. K.; Leung, C. W. T.; Lam, J. W. Y.; Tang, B. Z. Biosensing by luminogens with aggregation-induced emission characteristics. *Chem. Soc. Rev.* **2015**, *44*, 4228−4238.

(59) Hong, Y. N.; Lam, J. W. Y.; Tang, B. Z. Aggregation-induced emission: phenomenon, mechanism and applications. *Chem. Commun.* **2009**, *29*, 4332−4353.

(60) Zhang, H.; Cheng, L.; Nian, H.; Du, J.; Chen, T.; Cao, L. Adaptive chirality of achiral tetraphenylethene-based tetracationic cyclophanes with dual responses of fluorescence and circular dichroism in water. *Chem. Commun.* **2021**, *57*, 3135−3138.

(61) Xiong, J. B.; Feng, H. T.; Sun, J. P.; Xie, W. Z.; Yang, D.; Liu, M. H.; Zheng, Y. S. The Fixed Propeller-Like Conformation of Tetraphenylethylene that Reveals Aggregation-Induced Emission Effect, Chiral Recognition, and Enhanced Chiroptical Property. *J. Am. Chem. Soc.* **2016**, *138*, 11469−11472.

(62) Suresh, V. M.; De, A.; Maji, T. K. High aspect ratio, processable coordination polymer gel nanotubes based on an AIE-active LMWG with tunable emission. *Chem. Commun.* **2015**, *51*, 14678−14681.

(63) Lee, S.; Kim, K. Y.; Jung, S. H.; Lee, J. H.; Yamada, M.; Sethy, R.; Kawai, T.; Jung, J. H. Finely Controlled Circularly Polarized Luminescence of a Mechano-Responsive Supramolecular Polymer. *Angew. Chem., Int. Ed.* **2020**, *59*, 11697−11697.

(64) Duan, H. H.; Li, Y. W.; Li, Q. F.; Wang, P. P.; Liu, X. R.; Cheng, L.; Yu, Y.; Cao, L. P. Host-Guest Recognition and Fluorescence of a Tetraphenylethene-Based Octacationic Cage. *Angew. Chem., Int. Ed.* **2020**, *59*, 10101−10110.

(65) Qu, H.; Wang, Y.; Li, Z. H.; Wang, X. C.; Fang, H. X.; Tian, Z. Q.; Cao, X. Y. Molecular Face-Rotating Cube with Emergent Chiral and Fluorescence Properties. *J. Am. Chem. Soc.* **2017**, *139*, 18142−18145.

(66) Li, Y. W.; Dong, Y. H.; Cheng, L.; Qin, C. Y.; Nian, H.; Zhang, H. Y.; Yu, Y.; Cao, L. P. Aggregation-Induced Emission and Light-Harvesting Function of Tetraphenylethene-Based Tetracationic Dicyclophane. *J. Am. Chem. Soc.* **2019**, *141*, 8412−8415.

(67) Feng, H. T.; Yuan, Y. X.; Xiong, J. B.; Zheng, Y. S.; Tang, B. Z. Macrocycles and cages based on tetraphenylethylene with aggregation-induced emission effect. *Chem. Soc. Rev.* **2018**, *47*, 7452−7476.

(68) Brzechwa-Chodzynska, A.; Drozdz, W.; Harrowfield, J.; Stefankiewicz, A. R. Fluorescent sensors: A bright future for cages. *Coord. Chem. Rev.* **2021**, *434*, No. 213820.

(69) Mu, C. Q.; Zhang, Z. Y.; Hou, Y. L.; Liu, H. F.; Ma, L. Z.; Li, X. P.; Ling, S. L.; He, G.; Zhang, M. M. Tetraphenylethylene-Based Multicomponent Emissive Metallacages as Solid-State Fluorescent Materials. *Angew. Chem., Int. Ed.* **2021**, *60*, 12293−12297.

(70) Li, B.; He, T.; Shen, X.; Tang, D. T.; Yin, S. C. Fluorescent supramolecular polymers with aggregation induced emission properties. *Polym. Chem.* **2019**, *10*, 796−818.

(71) Tavakoli, J.; Ghahfarokhi, A. J.; Tang, Y. Aggregation-Induced Emission Fluorescent Gels: Current Trends and Future Perspectives. *Top. Curr. Chem.* **2021**, *379*, 9.

(72) Fang, H. B.; Cai, G. M.; Hu, Y.; Zhang, J. Y. A tetraphenylethylene-based acylhydrazone gel for selective luminescence sensing. *Chem. Commun.* **2018**, *54*, 3045−3048.

(73) Lu, C. J.; Zhang, M. M.; Tang, D. T.; Yan, X. Z.; Zhang, Z. Y.; Zhou, Z. X.; Song, B.; Wang, H.; Li, X. P.; Yin, S. C.; Sepehrpour, H.; Stang, P. J. Fluorescent Metallacage-Core Supramolecular Polymer Gel Formed by Orthogonal Metal Coordination and Host-Guest Interactions. *J. Am. Chem. Soc.* **2018**, *140*, 7674−7680.

(74) Konopka, M.; Cecot, P.; Ulrich, S.; Stefankiewicz, A. R. Tuning the Solubility of Self-Assembled Fluorescent Aromatic Cages Using Functionalized Amino Acid Building Blocks. *Front. Chem.* **2019**, *7*, 503.

(75) Jin, H. E.; Jang, J.; Chung, J.; Lee, H. J.; Wang, E.; Lee, S. W.; Chung, W. J. Biomimetic Self-Templated Hierarchical Structures of Collagen-Like Peptide Amphiphiles. *Nano Lett.* **2015**, *15*, 7138−7145.

(76) Hartgerink, J. D.; Beniash, E.; Stupp, S. I. Peptide-amphiphile nanofibers: A versatile scaffold for the preparation of self-assembling materials. *Proc. Natl. Acad. Sci. U. S. A.* **2002**, *99*, 5133−5138.

(77) Hartgerink, J. D.; Beniash, E.; Stupp, S. I. Self-assembly and mineralization of peptide-amphiphile nanofibers. *Science* **2001**, *294*, 1684−1688.

(78) Clarke, D. E.; Wu, G.; Wu, C.; Scherman, O. A. Further support comes from a recent work showing how rotation of a single amino acid within dipeptides lead to opposite CD signals, see: Host-Guest Induced Peptide Folding with Sequence-Specific Structural Chirality. *J. Am. Chem. Soc.* **2021**, *143*, 6323.

(79) Li, H.; Cheng, J.; Zhao, Y.; Lam, J. W. Y.; Wong, K. S.; Wu, H.; Li, B. S.; Tang, B. Z. L-Valine methyl ester-containing tetraphenylethene: aggregation-induced emission, aggregation-induced circular dichroism, circularly polarized luminescence, and helical self-assembly. *Mater. Horiz.* **2014**, *1*, 518−521.

(80) Li, H.; Cheng, J.; Deng, H.; Zhao, E.; Shen, B.; Lam, J. W. Y.; Wong, K. S.; Wu, H.; Li, B. S.; Tang, B. Z. Aggregation-induced chirality, circularly polarized luminescence, and helical self-assembly of a leucine-containing AIE luminogen. *J. Mater. Chem. B* **2015**, *3*, 2399−2404.

(81) Li, H.; Zheng, X.; Su, H.; Lam, J. W.; Sing Wong, K.; Xue, S.; Huang, X.; Huang, X.; Li, B. S.; Tang, B. Z. Synthesis, optical properties, and helical self-assembly of a bivaline-containing tetraphenylethene. *Sci. Rep.* **2016**, *6*, 19277.

(82) Li, H.; Yuan, W.; He, H.; Cheng, Z.; Fan, C.; Yang, Y.; Wong, K. S.; Li, Y.; Tang, B. Z. Circularly polarized luminescence and controllable helical self-assembly of an aggregation-induced emission luminogen. *Dyes Pigm.* **2017**, *138*, 129−134.

(83) Ono, K.; Iwasawa, N. Dynamic Behavior of Covalent Organic Cages. *Chem. − Eur. J.* **2018**, *24*, 17856−17868.

(84) Jacobson, H.; Stockmayer, W. H. Intramolecular Reaction in Polycondensations. I. The Theory of Linear Systems. *J. Chem. Phys.* **1950**, *18*, 1600−1606.

(85) Odian, G., *Principles of polymerization*, 4th ed. Wiley Interscience: Hoboken, New Jersey, 2004.

(86) Piazzolla, F.; Mercier, V.; Assies, L.; Sakai, N.; Roux, A.; Matile, S. Fluorescent Membrane Tension Probes for Early Endosomes. *Angew. Chem., Int. Ed.* **2021**, *60*, 12258−12263.

(87) Di, Q.; Li, J.; Zhang, Z.; Yu, X.; Tang, B.; Zhang, H.; Zhang, H. Quantifiable stretching-induced fluorescence shifts of an elastically bendable and plastically twistable organic crystal. *Chem. Sci.* **2021**, *12*, 15423−15428.

(88) Sakai, N.; Matile, S. Conjugated Polyimine Dynamers as Phase-Sensitive Membrane Probes. *J. Am. Chem. Soc.* **2018**, *140*, 11438−11443.